IV. Results

1. Western blot analysis of the expression of NCS proteins in peripheral tissues

VILIP-1 has been found mainly expressed in retinal (Lenz et al., 1992) and brain neurons (Saitoh et al., 1995; Lenz et al., 1996a; Bernstein et al., 1999, 2002, 2003; Hamashima et al., 2001; Spilker et al., 2002), but the expression profile of VILIP-1 in peripheral organs was still unknown, although VILIP-1 has been detected in the squamous carcinoma cells of the skin (Mahloogi et al., 2003). To investigate the distribution pattern of VILIP-1 in peripheral organs, we performed Western blot analysis with tissues of human and rat (Fig. 1 A) (Gierke et al., 2004).

Compared to brain tissue VILIP-1 showed a weaker but still strong reactivity in heart, lung, liver and testis and a weaker reactivity in ovary, kidney, spleen and pancreas. Besides in the brain, NCS-1 showed the strongest expression in the kidney, testis, ovary, and pancreas, and weaker expression in heart, liver and lung. In addition, we examined the protein expression pattern in rat tissues (Fig. 1 B and C). We further investigated the expression of those three NCS proteins in embryonic (E19) and adult (8 weeks) rat tissues. The strongest expression for VILIP-1 was seen in the embryonic tissue (Fig. 1 B) in heart, lung and testis. Additionally, we found strong expression in stomach and skin (not present on the human blot, compare Fig. 1 A and B). A weaker, but still detectable reactivity was observed in liver, spleen, kidney, pancreas and colon. In adult tissues a similar expression pattern was observed (Fig. 1 C); however, in comparison to the embryonic tissue, much less or no immunoreactivity appeared in liver, spleen, kidney, colon and pancreas.

Hippocalcin showed the highest expression levels in brain and virtually no expression could be detected in peripheral tissues in embryonic and adult tissues (Fig. 1 B and C). Besides expression in the brain, NCS-1 showed expression in most organs analyzed (Fig. 1 B and C). However, the highest expression levels occurred in the heart, kidney, and testis. Lower expression levels occurred in the lung, embryonic and adult tissues. Similar to VILIP-1 in adult tissues expression was reduced in some organs in particular in stomach, colon and skin or was lost completely in liver, lung and pancreas (Fig. 1 C). Therefore, the expression level became more comparable to the distribution in human tissue (compare Fig. 1 A and C) (Gierke et al., 2004).

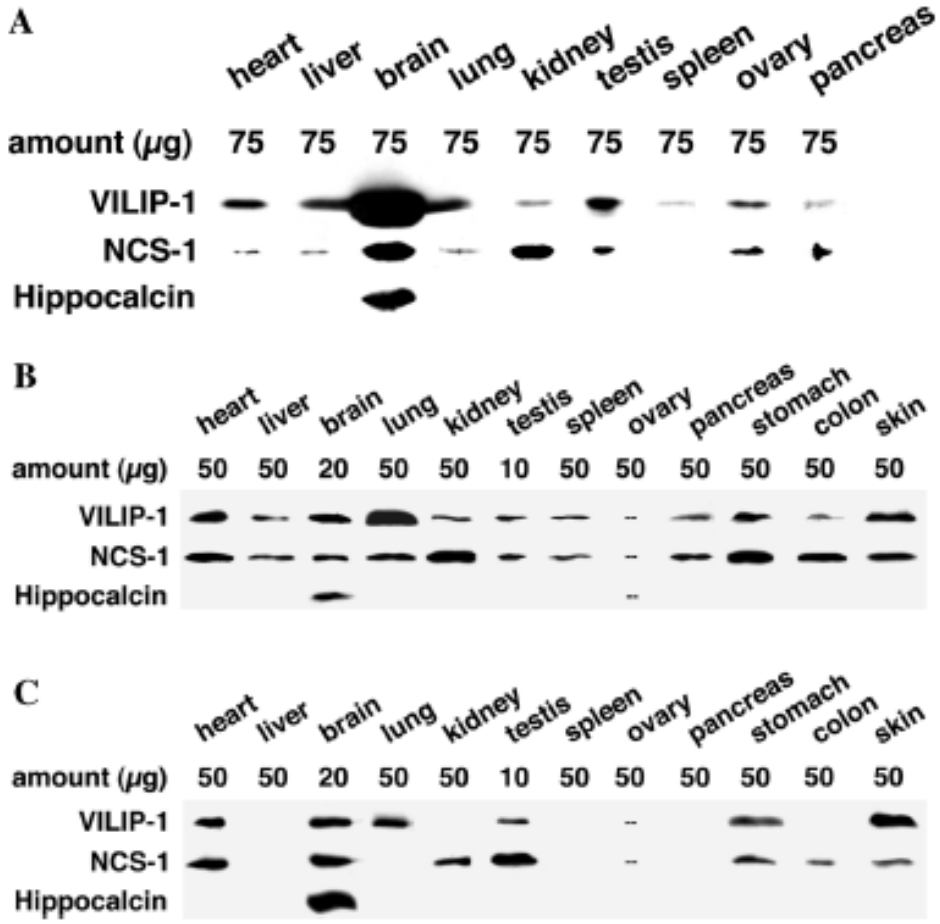

Figure 1 Western blot analysis of the expression of NCS proteins in brain and peripheral tissues of human and rat

Tissue expression of VILIP-1, Hippocalcin, and NCS-1 in Western blots of homogenates of different peripheral tissues such as heart, liver, brain, lung, kidney, testis, spleen, ovary and pancreas from human (A) and heart, liver, brain, lung, kidney, testis, spleen, ovary, pancreas stomach, colon and skin from rat embryonic (B) and rat adult (C) tissues. Western blots were probed with affinity-purified polyclonal antibodies against VILIP-1, Hippocalcin or polyclonal chicken antibodies against NCS-1. The amount of protein applied per lane is indicated.

2. Distribution of VILIP-1 in rat hippocampus

2.1. Overview of VILIP-1 expression in rat hippocampus

It was shown recently by *in situ* hybridization that VILIP-1 is highly expressed in all regions of the rat hippocampus (Paterlini et al., 2000). In addition, Bernstein et al. revealed that VILIP-1 was located in principal and some nonprincipal neurons of human and rat hippocampus. In the brains of schizophrenic patients and ketamine treated rats, VILIP-1 immunoreactivity in the hippocampal pyramidal cells was decreased, but VILIP-1 immunoreactivity in interneurons and the number of VILIP-1-immunoreactive interneurons was increased compared with healthy individuals (Bernstein et al., 2002, 2003). Changes in VILIP-1 expression were found in AD, cancer, and LTP neuronal plasticity (Braunewell, 2005). However, the precise function of

VILIP-1 is poorly understood and its distribution has not been studied extensively in rat hippocampus. Therefore, I further investigated the expression of VILIP-1 in rat hippocampus. VILIP-1-immunoreactivity (VILIP-1-IR) was found exclusively in hippocampal neurons, where it coexisted with the neuronal marker NeuN in the subregion CA1 (cornu ammonis 1), CA3 (cornu ammonis 3), and dentate gyrus (DG) of the hippocampus (Fig. 2 A, B, C) but not in astrocytes, which are GFAP immunopositive in different subregions of the hippocampus (Fig. 2 D, E, F).

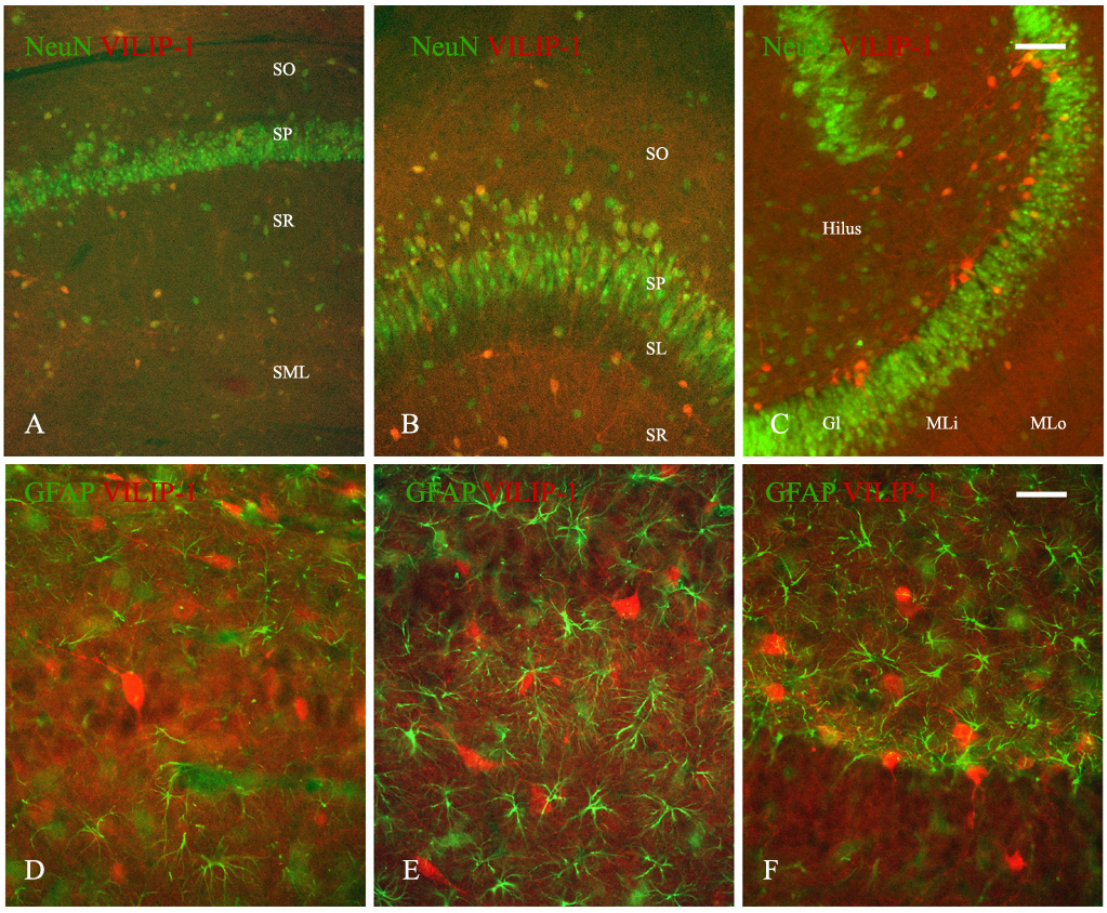

Figure 2 Co-localization of VILIP-1 with the neuronal marker NeuN but not the astrocyte marker GFAP.
Co-staining of VILIP-1 and NeuN (A, B, C); VILIP-1 and GFAP (D, E, F) in hippocampal CA1 (A, D), CA3 (B, E), and dentate gyrus (C, F). VILIP-1-IR cells are always positive for NeuN, but GFAP containing cells never show VILIP-1 immunoreactivity. gl, granular layer; sl, stratum lucidum; sml, stratum lacunosum-moleculare; sp, stratum pyramidale; so, stratum oriens; sr, stratum radiatum; MLo, outer molecular layer; MLi, inner molecular layer. Scale bar: C 100µm, F 50µm.

VILIP-1-IR cells were diverse in size and morphology. Moderate VILIP-1 immunoreactivity was seen in most hippocampal principal cells (Fig. 3 A). The somata and dendrites were both immunoreactive in hippocampal CA3 region, and dentate gyrus, and diffuse distribution of VILIP-1 immunoreactivity was seen in the somata of the cells (Fig. 3). Note the intense immunoreactivity in Schaffer collateral fibers of CA1, and the fibers located in the stratum

radiatum and lacunosum-moleculare of CA3. Immunostaining for VILIP-1 are shown in different layers of CA1 (Fig. 3 B), CA3 (Fig. 3 C), dentate gyrus (Fig. 3 D). Note that another strong VILIP-1-IR cell in stratum radiatum was seen, with a long process ending in the stratum oriens of CA1 (Fig. 3 B). Furthermore, axonal arborizations and terminal fields of immunoreactive boutons were stained strong enough to be clearly visualized in some cases (Fig. 3 B and inset, C, D). Moreover, to some extent the dendritic tree was also revealed. In the CA1 and CA3 region, pyramidal cells (Fig. 3) have moderate stained long and barely arborized dendrites running into the stratum radiatum. The immunoreactive dendrites in the stratum radiatum and the stratum lacunosum moleculare of CA3 are stronger than in CA1. In the dentate gyrus (DG), most granule cells were immunoreactive except the neurons in the subgranular zone (SGZ) (Fig. 3 A, D). Some intensely VILIP-1-IR nonprincipal cells were scattered in the different hippocampal subfields, including in the stratum oriens, radiatum and lacunosum-moleculare of CA1, CA3, and the hilus of the dentate gyrus, with regard to their morphological and localization characters. The hilus contains large, intensely stained neurons with immunoreactive processes, especially in the hilar border, being much less abundant in the hilus and in the molecular layer (Fig. 3 D). Some typical pyramidal-like VILIP-1-IR neurons were also seen in the hilar border of the granule cell layer.

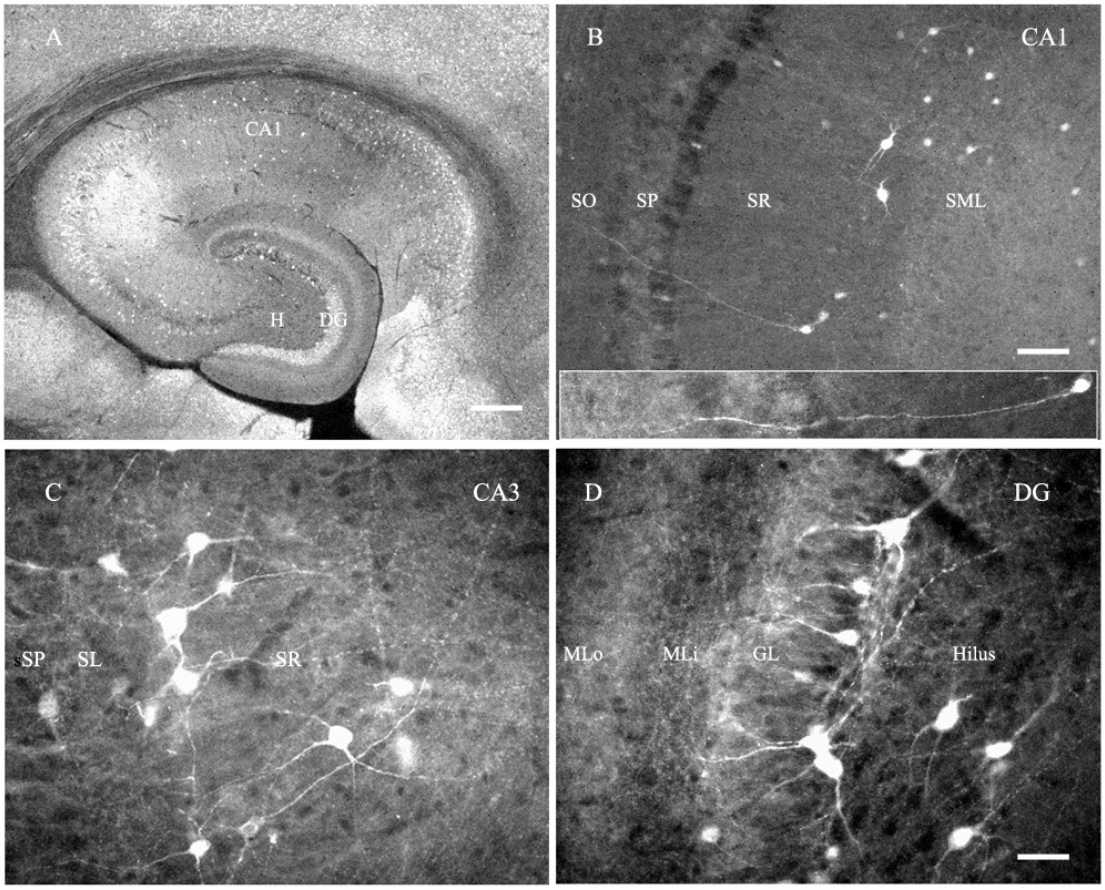

Figure 3 VILIP-1-IR cells in the rat hippocampus
A: Overview of VILIP-1-IR cells distribution. Weak or moderate immunoreactive cells were mainly located in principal cell layers, and some intense immunoreactive cells could be seen in nonprincipal cells regions. B: two big horizontal fusiform VILIP-1-IR cells were located in the stratum radiatum of CA1. C: VILIP-1-IR cells located in CA3 were multipolar or fusiform. D: VILIP-1-IR cells in the dentate gyrus. In hilar border and hilus, some pyramidal like cells could be seen. H. hilus; gl, granular layer; sl, stratum lucidum; sml, stratum lacunosum-moleculare; sp, stratum pyramidale; so, stratum oriens; sr, stratum radiatum; MLo, outer molecular layer; MLi, inner molecular layer. Scale bar: A, 250μm, B, 100μm, D, 50μm.

2.2. Co-localization of VILIP-1 with GABAergic neuronal marker GAD67

Given that astrocytes do not express VILIP-1, the morphological character and localization of the intense immunoreactive VILIP-1 cells suggested that those VILIP-1-IR cells are likely to be interneurons. We further demonstrated that VILIP-1-IR neurons are a subpopulation of GABAergic interneurons by immunofluorescence co-staining of the GAD67 and VILIP-1. GAD67-containing interneurons were observed in all subfields of the CA1, CA3 and dentate gyrus (Fig. 4 D, E, F). Normally, large immunoreactive somata were seen in the stratum radiatum and border of hilus, and only a part of VILIP-1-IR nonprincipal neurons were present in strong GAD67 immunoreactivity (Fig. 4 arrows). Since GAD67 is present in somata and axon terminals, weak GAD immunoreactivity in somata does not necessarily indicate the scarcity of GAD molecules throughout their intracellular space (Fukuda et al., 1997). Therefore, more specific and sensitive neurochemical interneuron markers co-staining with VILIP-1 were applied in further experiments.

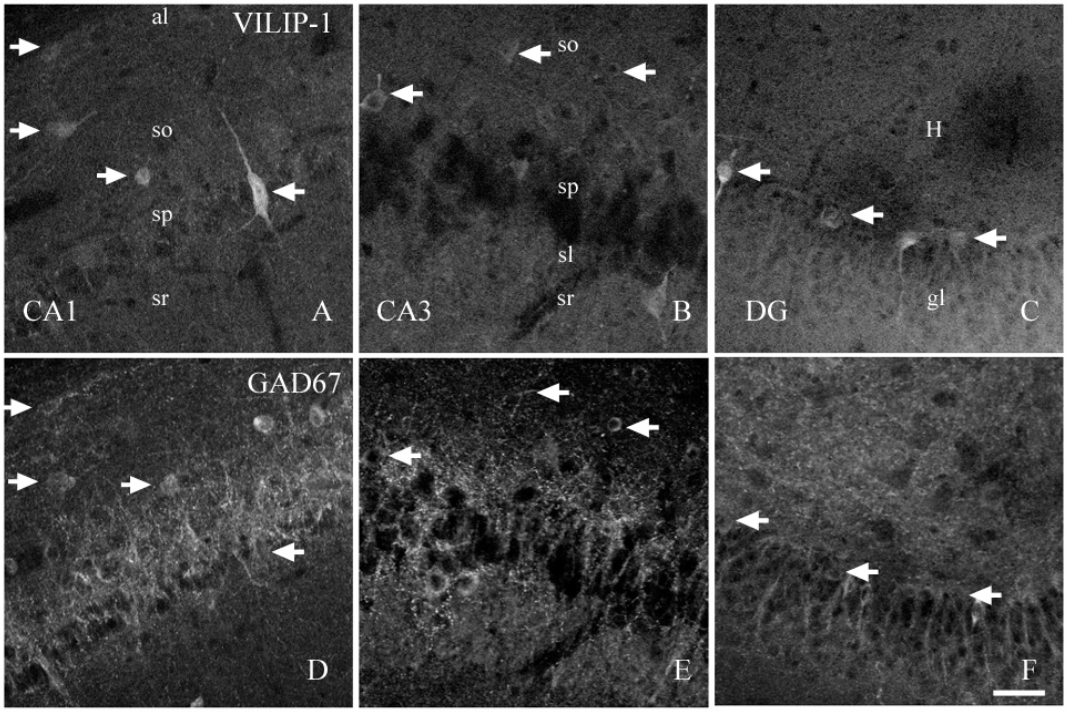

Figure 4 Co-localization of VILIP-1 with GABAergic neuron marker GAD67

Representative co-stainings of VILIP-1 (A, B, C) and GAD67 (D, E, F), in hippocampal CA1 (A, D), CA3 (B, E) and dentate gyrus (C, F). Most VILIP-1-IR cells were positive for GAD67, but the GAD67 immunoreactivity was relatively weak. Note some GAD67-IR cells which did not contain VILIP-1. gl, granular layer; sl, stratum lucidum; sp, stratum pyramidale; so, stratum oriens; sr, stratum radiatum. Scale bar: 50µm.

2.3. Co-localization of VILIP-1 with Parvalbumin (PV)

Parvalbumin (PV) was filled in the somata, the entire dendritic tree and axon terminals of exclusively nonprincipal cells. Most PV-IR neurons were seen in the stratum oriens and pyramidale of the CA1, CA3 regions, and adjacent to the stratum granulosum of the dentate gyrus (Fig. 5 D, E, F). PV-IR interneurons were seen in stratum pyramidale and oriens in the CA1 area. A few PV-IR cells in the stratum oriens and stratum pyramidale of CA1, CA3 and the border of the hilus were co-localized with VILIP-1. This finding was similar to the study using PV-GFP transgenic mice (data not shown). This observation was in line with previous findings of a limited co-localization of VILIP-1 with approximately 10% of the PV-IR interneurons in human brain (Bernstein et al., 1999).

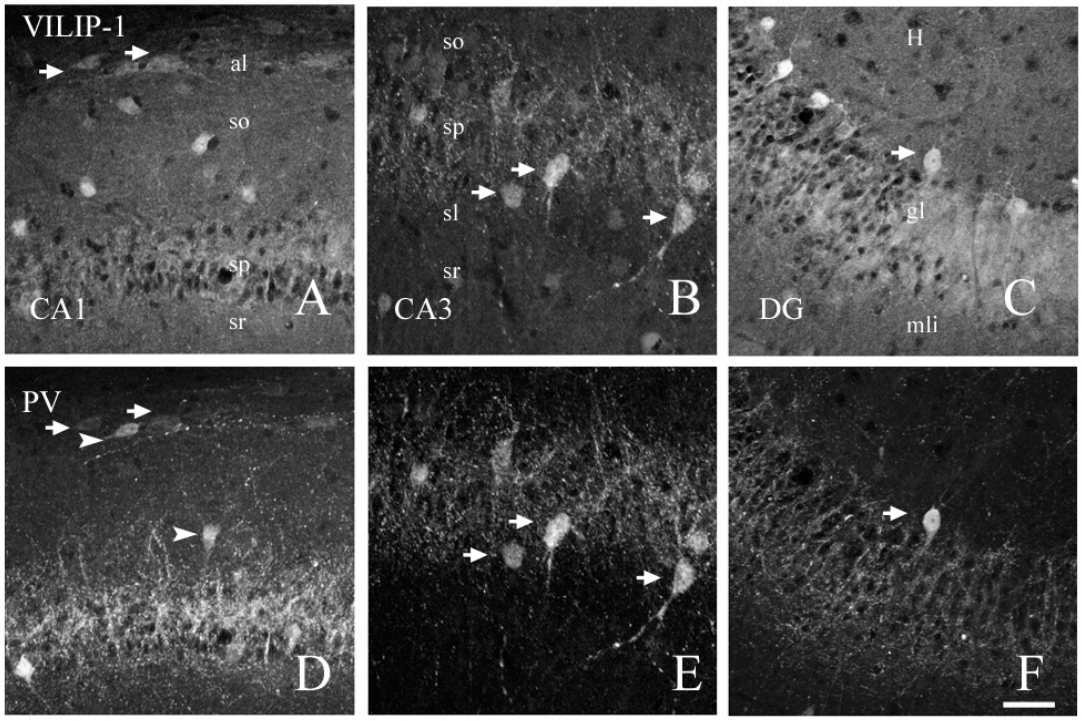

Figure 5 Co-localization of VILIP-1 with Parvalbumin (PV)
Representative co-stainings of VILIP-1 (A, B, C) and PV (D, E, F) are shown, in hippocampal CA1 (A, D), CA3 (B, E) and dentate gyrus (C, F). In the CA3 region, PV-IR interneurons were present in all layers, except in the stratum lacunosum-moleculare. In the dentate gyrus, PV-IR cells could be found within or adjacent to the stratum granulosum, occasionally PV-containing interneurons could be observed in the hilus and stratum moleculare. Most VILIP-1-IR cells were negative for PV, but in the alveus, stratum oriens and pyramidal layer and the border of the hilus, a few VILIP-1-IR cells containing PV could be found. al, alveus; gl, granular layer; sl, stratum lucidum; sp, stratum pyramidale; so, stratum oriens; sr,

stratum radiatum; MLi, inner molecular layer. Scale bar: 50µm

2.4. Co-localization of VILIP-1 with Calbindin-D28k

Calbindin-D28k-immunopositive cells with filled somatic and dendritic cytoplasm were found in both principal and non-principal cells in the hippocampus. Among the principal cells the granule cells of the dentate gyrus and the superficial pyramidal cells of the CA1 region were found to be Calbindin-D28k-immunoreactive (Calbindin-D28k-IR) (Fig. 6 D, F). The pyramidal cells of the CA3 region were immunonegative, but the intense immunoreactive mossy fibers, the axons of granule cells, were also visible (Fig. 6 E). The Calbindin-D28k-IR interneurons scattered in the stratum oriens, radiatum and the border of the stratum radiatum and lacunosum-moleculare in the CA1. Most VILIP-1 and Calbindin-D28k co-localized interneurons were found in the stratum radiatum of CA1 (Fig. 6 A, D, arrows). In CA3, Calbindin-D28k-IR interneurons were found in the stratum radiatum, and also the lucidum but less frequently in the stratum oriens and moleculare (Fig. 6 E). Similar to CA1, most co-localized neurons were seen in the stratum radiatum of CA3, but co-localization was also seen in the stratum lucidum. In the dentate gyrus, most Calbindin-D28k-IR interneurons were located at the border of the stratum granulosum and the hilus, less in the stratum moleculare. Calbindin-D28k-IR interneurons containing VILIP-1 were mainly seen in these areas as well (Fig. 6 C, F). Because of the immunoreactivity of granule cells, the Calbindin-D28k-IR interneurons in the granular layer were difficult to be identified.

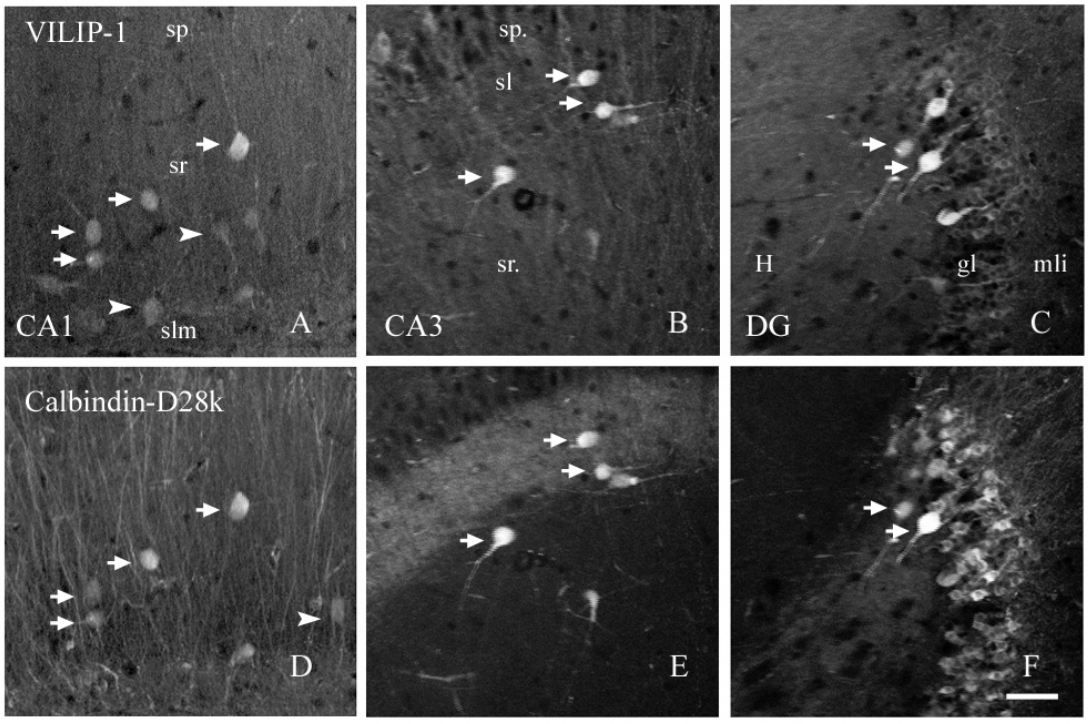

Figure 6 Co-localization of VILIP-1 with Calbindin28kD (Calbindin-D28k)
VILIP-1 (A, B, C) and CB (D, E, F), corresponding to CA1 (A, D), CA3 (B, E) and dentate gyrus (C, F), both principal cells and interneurons, contained Calbindin-D28k. In the CA1 area (B), superficial pyramidal cells and interneurons were Calbindin-D28k-IR. In the CA3 region (E), Calbindin-D28k-IR interneurons located in the Calbindin-D28k-negative pyramidal layer, whereas moderate Calbindin-D28k-IR mossy fibers were clearly visible in the stratum lucidum. In the dentate gyrus, granule cells and interneurons in the hilar border showed Calbindin-D28k-IR. Some VILIP-1-IR cells were positive for Calbindin-D28k; Note some Calbindin-D28k-IR cells which do not contain VILIP-1. H, hilus; gl, granular layer; sl, stratum lucidum; sp, stratum pyramidale; so, stratum oriens; sr, stratum radiatum; slm, stratum lacunosum-moleculare; MLi, inner molecular layer. Scale bar: 50μm.

2.5. Co-localization of VILIP-1 with Calretinin (CR)

Calretinin (CR) is present in the somata, proximal and distal dendrites and axons of nonprincipal neurons. Calretinin-immunoreactive (CR-IR) interneurons scattered in all layers. In the CA1 and CA3 regions, CR-IR cells were multipolar, bipolar, or fusiform and were found in all layers (Fig. 7 D, E). CR-IR cells were located in the stratum radiatum, pyramidale and oriens. About 50% of CR-IR cells were VILIP-1 immunoreactive in various subfields of CA1 and CA3 (Fig. 7 A, B, D, and E). In the dentate gyrus, most CR-IR cells were located at the border of the hilus. Some of them often have pyramidal-shaped somata which mostly contain VILIP-1. In the stratum molecular and in the hilus, multipolar and bipolar cells were seen showing morphological features of interneurons. Thus, calretinin was found to be the best marker to characterize VILIP-1 expression in a defined subpopulation of presumably interneurons in the rat hippocampus.

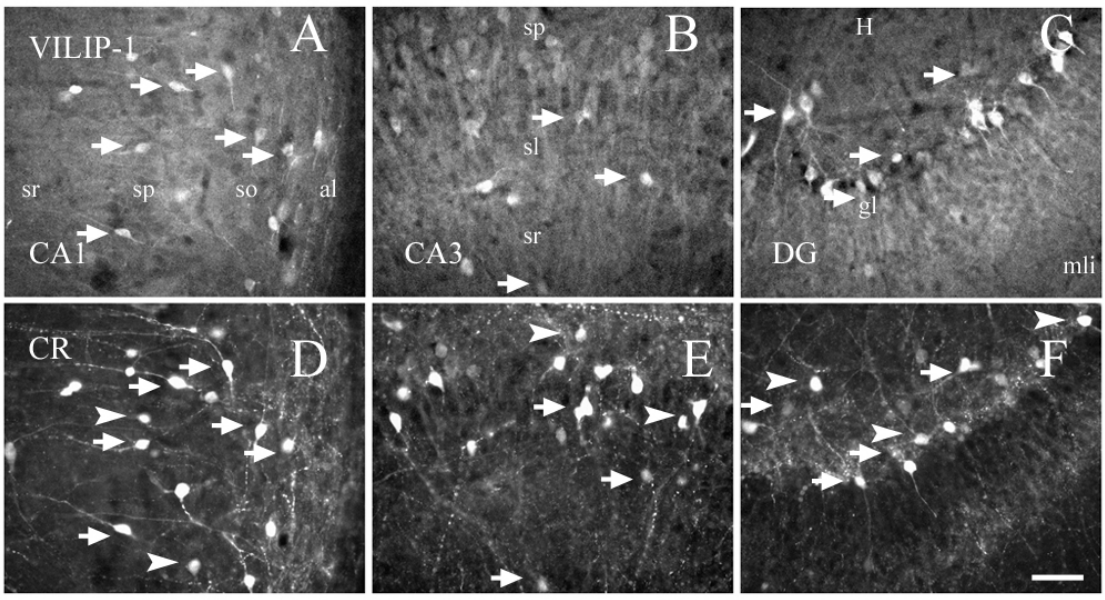

Figure 7 Co-localization of VILIP-1 with Calretinin (CR)
Representative co-stainings of VILIP-1 (A, B, C) and CR (D, E, F), in hippocampal CA1 (A, D), CA3 (B, E) and dentate gyrus (C, F). Calretinin scattered in non-pyramidal cells in all areas and layers of the hippocampal formation, and in the hippocampal fissure. There were high intense immunoreactive cell bodies and dendrites in the hilus of the dentate gyrus and in the stratum lucidum of the CA3 area. Most VILIP-1-IR cells were positive for CR. Note some CR-IR cells which do not contain VILIP-1. H, hilus; gl,

granular layer; sl, stratum lucidum; sp, stratum pyramidale; so, stratum oriens; al, alveus; sr, stratum radiatum; MLi, inner molecular layer. Scale bar: 50μm.

2.6. Co-localization of VILIP-1 with mGluR1α

In the rat hippocampus, mGluR1α-immunoreactive (mGluR1α-IR) elements included the somata and dendrites of non-principal cells. The mGluR1α-IR cells in CA1 were abundant at the border of the stratum oriens and the alveus (Fig. 8 D). A horizontally oriented or multipolar, spiny dendritic tree was usually seen. In other layers, a few weak immunoreactive cell bodies were observed, and they showed a multipolar morphology (Fig. 8 D, E, F). In the stratum lacunosum-moleculare, mGluR1α-IR profiles were rarely seen. The strong co-localization between VILIP-1 and mGluR1α was mainly found in the stratum oriens and the alveus of CA1.

In the CA3 area, most immunopositive cells could be found in the stratum oriens bordering the alveus as well (Fig. 8 E). Weak mGluR1α-IR cells could be found in all other layers (Fig. 8 E). They showed varied appearances, with radially oriented, horizontal or multipolar aspiny or sparsely spiny dendrites. The stratum lacunosum-moleculare possessed a very small number of immunoreactive elements. Similar to CA1, co-localization between VILIP-1 and mGluR1α was found in the stratum oriens and the alveus of CA3. In the dentate gyrus, mGluR1α-IR cells had a multipolar dendritic tree in the deep hilus (Fig. 8 F). These spiny dendrites were typically restricted to the hilus. Only a few neurons contained both markers. Thus, particularly large interneurons located in the stratum oriens/alveus of CA1 and CA3 subregions were found to show strong co-localization of VILIP-1 and mGluR1α-IR.

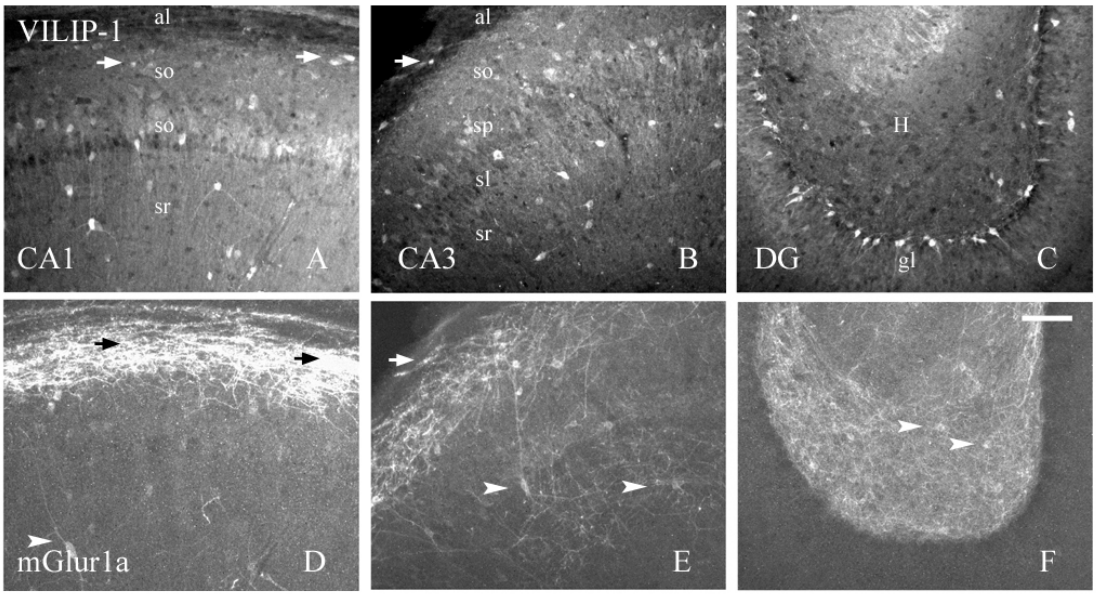

Figure 8 Co-localization of VILIP-1 with mGluR1α
VILIP-1 (A, B, C) and mGluR1α (D, E, F) in hippocampus subregions, CA1 (A, D), CA3 (B, E) and dentate gyrus (C, F). Intense immunoreactive mGluR1α cell bodies and dendrites were seen in the alveus and stratum oriens of the CA1, CA3, which partly coexist with VILIP-1. In addition, some weak immunoreactive cell bodies and dendrites also could be found in the stratum radiatum of CA1, CA3 and

the hilus of the dentate gyrus, with negative immunoreactivity for VILIP-1. H, hilus; gl, granular layer; sl, stratum lucidum; al, alveus; so, stratum oriens; sp, stratum pyramidale; sr, stratum radiatum. Scale bar: 100μm.

2.7. Co-staining of VILIP-1 with PSA-NCAM

It was reported that the newly born granule cells of the subgranular zone (SGZ) transiently express CR in the mouse hippocampus, which can be identified by other markers, for instance, PSA-NCAM (polysialylated forms of the cell-surface glycoprotein NCAM), Doublecortin (DCX) (Brandt et al., 2003; Kempermann et al., 2004). Therefore, VILIP-1 and PSA-NCAM co-staining was performed in rat hippocampal slices to distinguish whether VILIP-1/CR-IR cells located in hilar border are newly born cells or not. Neither VILIP-1 immunoreactivity (Fig. 9 D, F) nor CR immunoreactivity (Fig. 9 A, C) was found in the newly born cells of SGZ in rat hippocampus, opposite to the finding that CR but not VILIP-1 was seen in newly born cells coexisting with PSA-NCAM in similar experiments performed on mouse slices (data not shown).

Thus, VILIP-1-IR seems to be restricted to CR-IR interneurons in the dentate gyrus, and does not seem to be expressed in newly born granule cells. This is in contrast to that moderate or weak VILIP-1-IR was found in mature granule cells in the rat dentate gyrus in present study (Fig 3), which is consistent with previous finding (Bernstein et al., 2003).

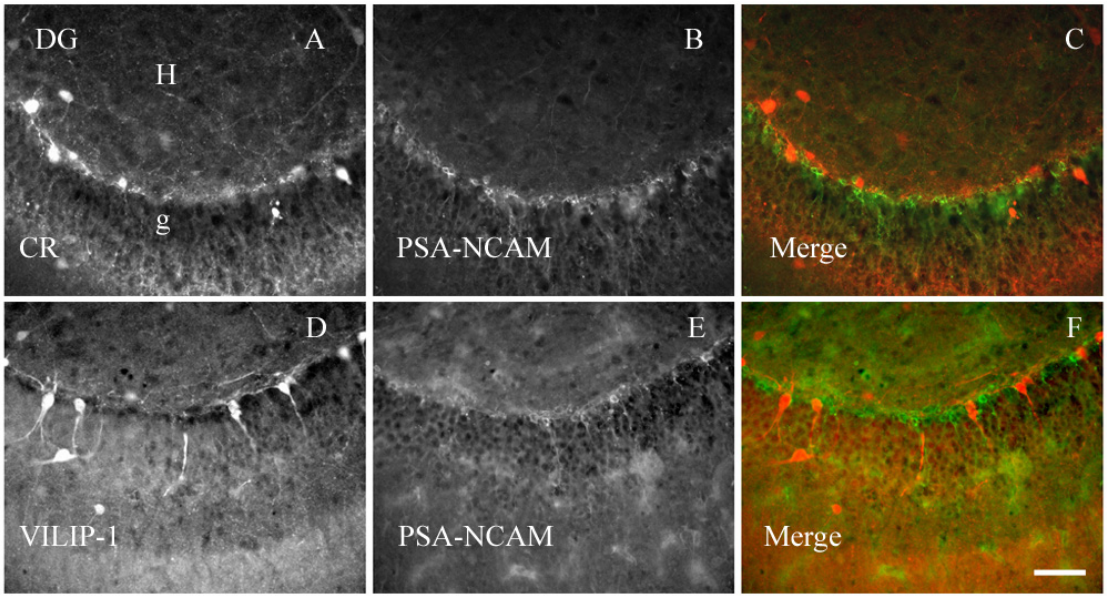

Figure 9 Co-staining of VILIP-1 and CR with PSA-NCAM
Either VILIP-1immunopositive cells (D, F) or CR immunopositive cells (A, C) were exclusive to PSA-NCAM immunopositive newly born neurons (B, E respectively) which were located in the subgranular zone (SGZ) of the dentate gyrus. H, hilus; g, granular layer. Scale bar: 60μm.

2.8. VILIP-1 and α4β2 nAChR show partial co-localization in hippocampal neurons

VILIP-1 interacts with the α4 nAChR subunit, and enhances surface and functional expression of α4β2 nAChR in oocytes (Lin et al., 2002). In order to study the significance of the effect of VILIP-1 on surface expression and functional up-regulation of α4β2 nAChR *in vitro*, we

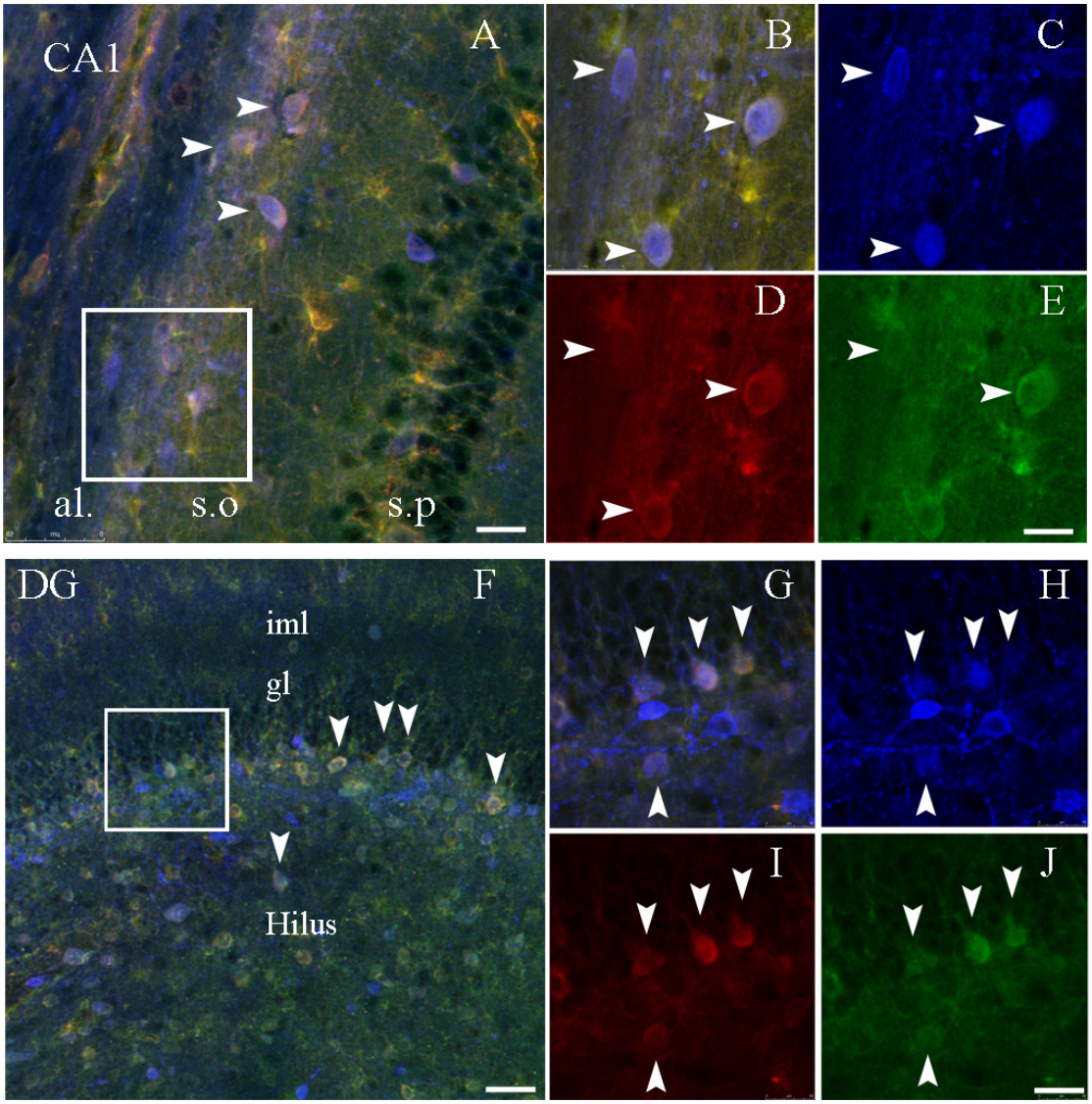

Figure 10 VILIP-1 and α4β2 nAChR show partial co-localization *in vitro* in hippocampal slices.
Immunohistochemical co-staining experiments (A, F) with antibodies against the α4-subunit of the α4β2 nAChR complex (both red channel and green channel), and VILIP-1 (blue channel) were shown in hippocampal slices. The co-staining is visible in a subset of neurons representing hippocampal principal cells and interneurons in the CA1 regions (arrows in A) and the dentate gyrus (arrows in F). Combined staining of two commercial antibodies directed against different receptor epitopes (mab299, red channel, mab α4, green channel) with polyclonal antibodies against VILIP-1 (blue channel) revealed clear co-staining in white in neurons in the CA1 and dentate gyrus (A, F). al, alveus; sp, stratum pyramidale; so, stratum oriens; gl, granular layer; MLi, inner molecular layer. Bar in A, F is 40 µm; Bar in E, J is 20 µm.

performed immunohistochemical co-staining experiments with antibodies against the α4-subunit of the α4β2 nAChR complex and against VILIP-1 in hippocampal slices of rat (Fig. 10). The

protein expression of both markers showed some differences in their expression pattern, but clear co-localization was noticeable in a subset of neurons mainly representing hippocampal interneurons in the CA1 regions (Fig. 10 A-E) and the dentate gyrus (Fig. 10 F-J). To increase the specificity for the antibodies against the α4-subunit of the α4β2 nAChR and to reduce background staining, we combined staining of two commercial antibodies directed against different receptor epitopes. Triple staining of the two antibodies with VILIP-1 revealed clear triple co-staining in white in distinct neurons in the hippocampal CA1 region and the dentate gyrus. As identified by morphological means many of the co-stained neurons represent interneurons, for example, in the stratum oriens, pyramidale and moleculare in the CA1 region (Fig. 10 A-E, arrows) and in hilus interneurons and in interneurons bordering the granule cell layer in the dentate gyrus (Fig. 10 F-J, arrows). These results indicate that VILIP-1 and its interaction partner α4β2 nAChR co-localize in a specific subset of neurons in the rat hippocampal formation, particularly interneurons.

Since partial co-localization of VILIP-1 and α4β2 nAChR was demonstrated in rat hippocampal tissue *in vitro*, I was interested in whether the influx of Ca^{2} via α4β2 nAChR can lead to the conformation change of VILIP-1, exposure of the myristoylation motif and translocation of VILIP-1 to the membrane complex. Therefore, to study VILIP-1 translocation during the influx of Ca^{2+} via endogenous nAChRs, primary hippocampal neurons (DIV14 in culture) which at that time had reached stage 5 of differentiation according to Goslin and Banker (Goslin and Banker, 1998) were used in the following experiment.

3. Localization of endogenously expressed VILIP-1 in cultured hippocampal neurons and translocation to the plasma membrane after physiological stimulation

Spilker et al. (Spilker et al., 2002) demonstrated the activity-dependent subcellular localization of VILIP-1 induced by a rise in intracellular calcium triggered by glutamate. To set up the VILIP-1 translocation experiment, hippocampal neurons were stimulated with 100 µM glutamate/10 µM glycine for 30 seconds, 1 min, and 2 min, respectively, before fixation. The cells were labeled with the preabsorbed polyclonal VILIP-1 antibody alone or and a polyclonal antibody against alpha4 nAChR. Endogenous VILIP-1 is heterogeneously expressed in hippocampal neurons and is distributed throughout the cell in the somata, as well as in neuritic processes (Fig. 13 I). Glutamate induced an enrichment of fluorescence in intracellular structures, at the plasma membrane, and along dendritic processes (Fig. 11 D, E, F. Fig. 12 middle lane). The translocation occurred rapidly, and clear changes in localization were seen within 30 sec (data not shown), VILIP-1 reached a maximum redistribution within 2 minutes after drug incubation (Fig. 11 D, E, F; Fig. 12 middle lane, red channel). These results indicate that an activity-dependent and calcium-mediated translocation to the cell surface membrane of

hippocampal neurons around the soma and to distinct sites of dendritic membranes can be observed for endogenously expressed VILIP-1 in hippocampal neuron cultures.

Similar to the effect of glutamate, translocation of endogenous VILIP-1 after 5µM nicotine incubation for 30 seconds, 1 minute, and 2 minutes could be seen in hippocampal cultured neurons. Translocation could be detected more easily at the 2 minute time point of incubation (Fig. 11G, H, I; Fig. 12 low of lane, red channel), together with the previous data; I presented all data at 2 minutes, and selected this time point for the experiment. Quantification of the relative VILIP-1 fluorescence intensity was shown in the inset of Fig. 11.

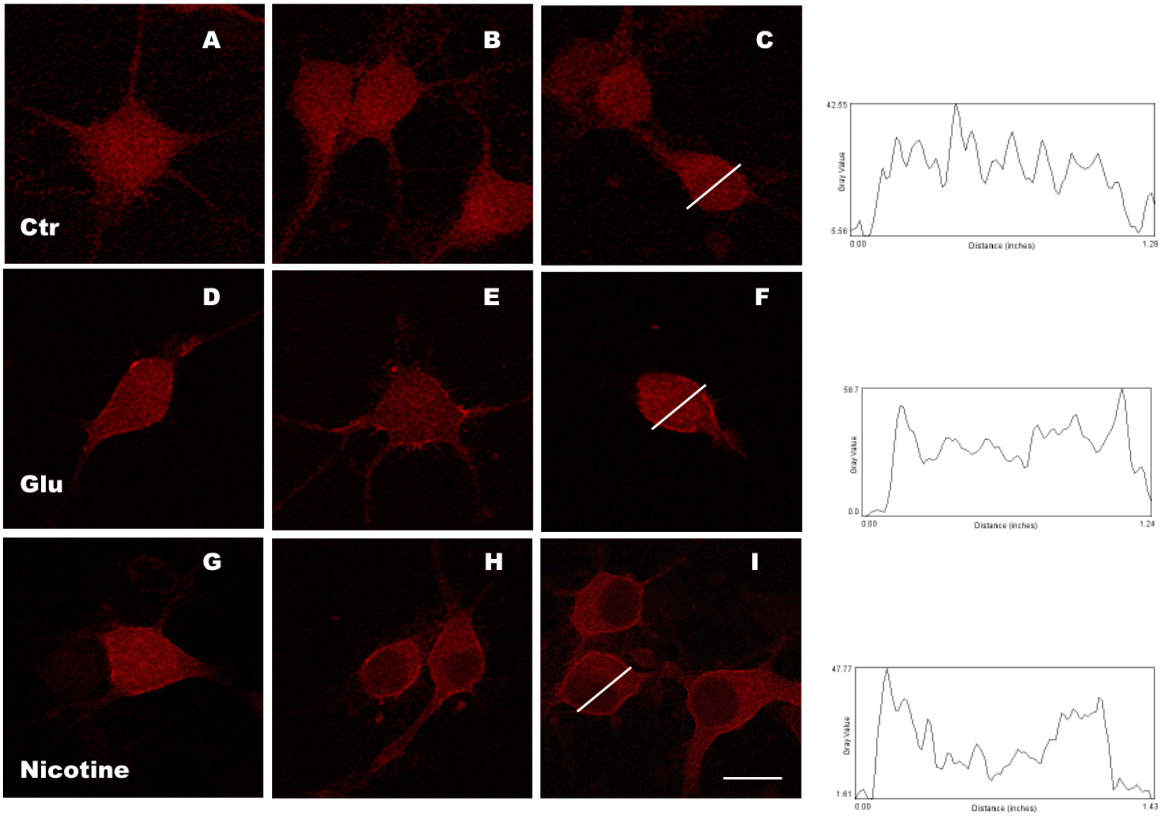

Figure 11 Confocal images show the translocation of endogenous VILIP-1 in cultured hippocampal neurons after a physiological stimulus.
The insets show the quantification of the pixel values (relative VILIP-1 fluorescence intensity) from a cross section of the shown neurons as indicated with the white bars. The peaks at the edges of the curve of the insets indicate the localization of the cell surface membrane. Scale bar: 10 µm.

Co-localization of VILIP-1 with the α4 nAChR subunit could be seen in some hippocampal neuron culture, which suggests the α4β2 nAChR subunit might also contribute to the nicotine triggered translocation of VILIP-1. I further demonstrated nicotine triggered translocation of VILIP-1 could be inhibited by preincubation with EGTA (Fig. 13 D, E, F), which confirmed the findings of Spilker et al. (Spilker et al., 2002) that external Ca^{2+} is essential for translocation of VILIP-1. In addition, the translocation of VILIP-1 induced by incubation of nicotine was

abolished after adding EGTA (Fig. 13 J, K, and L), which further confirmed that translocation of VILIP-1 is reversible in cultured hippocampal neurons (Spilker et al., 2002).

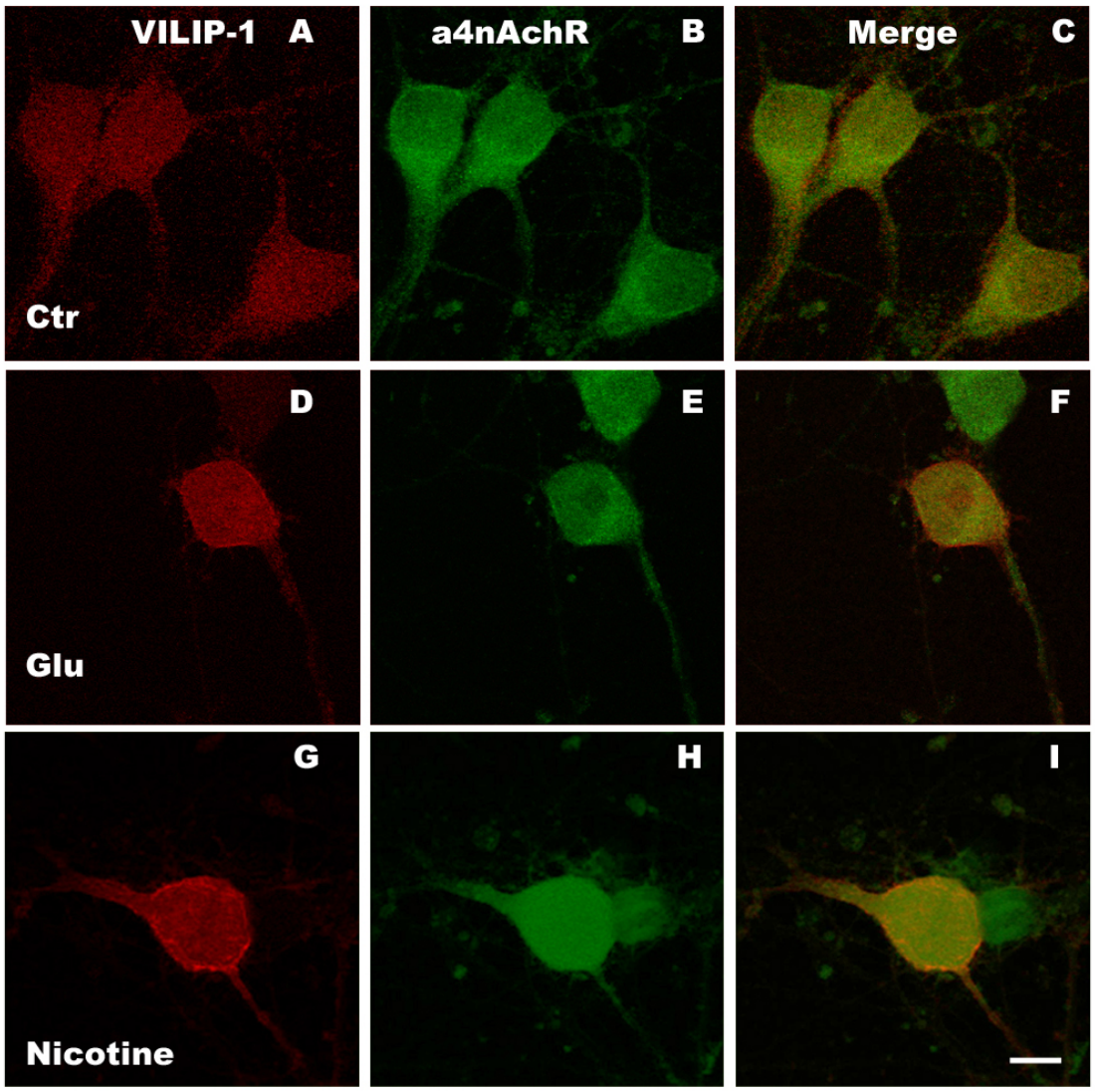

Figure 12 Confocal image demonstrates the coexistence of endogenous α4 nAChR subunit and endogenous VILIP-1, and translocation of VILIP-1 after a physiological stimulus in cultured hippocampal neurons.
Rat hippocampal neurons grown on glass coverslips were fixed after 2 weeks in culture and labeled with polyclonal anti-VILIP-1 antibodies and secondary Cy3 anti-rabbit antibodies (red channel) and polyclonal anti-nAChR antibodies and secondary Alexa Fluor 488 anti-mouse antibodies (green channel). Merged images of red (Cy3) and green (Alexa Fluor 488) fluorescence are shown in left column. Double-stained primary neurons incubated with 5μM nicotine for 2 minutes before fixation show strong labeling of the plasma membrane (arrows) around the soma with red VILIP-1 fluorescence coincidently labeled with green anti-nAChR fluorescence. Bar scale: 10 μm.

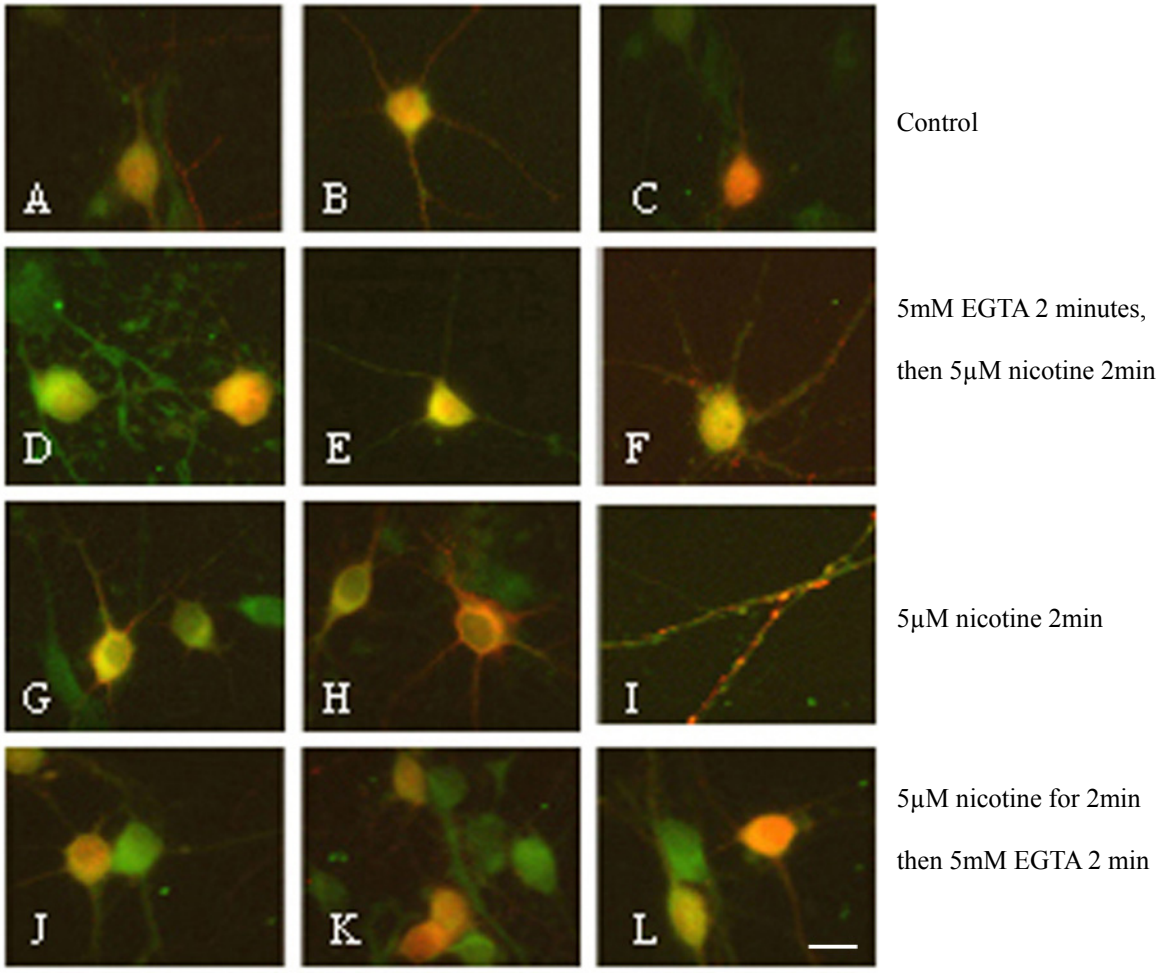

Figure 13 Characterization of the translocation of endogenous VILIP-1 in hippocampal neuron culture *in vitro.*

Representative examples of the translocation of VILIP-1 are shown as co-staining with polyclonal anti-VILIP-1 antibodies (red channel) and polyclonal anti-nAChR antibodies (green channel) after incubation of 5µM nicotine for 2 minutes (G, H, I), compared to the control conditions (A, B, C). Inhibition of the effect of nicotine by preincubation of EGTA is demonstrated in D, E, F, reversal membrane distribution of endogenous VILIP-1 is shown in J, K, and L. Bar 10µm**.**

4. Effect of nicotine stimulation on VILIP-1 α4β2 nAChR co-localization: comparison of translocation of VILIP-1 induced by the activation of nAChR and ionotropic glutamate receptor

I compared the translocation of VILIP-1 induced by the nAChR activation with the effect of the ionotropic glutamate receptor channel activation, a highly Ca^{2+}-permeable channel. An increase in the intracellular calcium concentration of cultured hippocampal neurons was achieved by adding 5µM nicotine. In neurons, 5µM nicotine induced an enrichment of VILIP-1 fluorescence in intracellular structures, at the plasma membrane, which is similar to the effect of glutamate (Fig. 13).

Pretreatment of unstimulated cells with EGTA significantly reduced the translocation of VILIP-1 induced by 5μM nicotine (Fig. 13 D, E, and F), which suggested calcium is essential for VILIP-1 translocation to the membrane. Furthermore, when cells undergoing translocation of VILIP-1 were treated with 5 mM EGTA, which specifically chelates Ca^{2+}, the translocation process was completely inhibited within 2 minutes (Fig. 13 J, K, and L). Although the initial Ca^{2+} peak is due to calcium release from the intracellular stores, the continuous elevation in Ca^{2+} levels requires Ca^{2+} influx, which can be effectively blocked by chelation with EGTA (Hartmann and Verkhratsky, 1998; Losavio and Muchnik, 2000; Meine et al., 1994). These results indicate that VILIP-1 can calcium-dependently localize to different subcellular compartments, also suggesting that the calcium–myristoyl switch of VILIP-1 occurs in living cells and can function in both directions, as previously described (Spilker et al., 2002).

The effect of non-α7 nAChRs was examined. To selectively activate non-α7 nAChRs, MLA (1 nM) was incubated for 15 minutes to block α7 receptors, and then 5μM nicotine was incubated for 2 minutes, the effect of nicotine dramatically decreased （about 16.4%） compared to the effect (57.6%) in the control mediated by all nAChR including α7 nAChR (Fig. 14). This suggests that α7 nAChR evoked by 5μM nicotine contributes most to the increase of intracellular Ca^{2+}. This finding was further confirmed by preincubation of 1nM MLA (methylallylaconitine) /100nM DHβE (dihydro-beta-erythroidine, Sigma) for 15 minutes, which only slightly further decreased the translocation of VILIP-1 compared with MLA (1nM) alone. However translocation of VILIP-1 evoked by glutamate was not attenuated by either MLA or MLA/DHβE. This suggested that the activation of α7 nAChRs significantly increases the Ca^{2+} level in most hippocampal neurons (Fig. 14), compared to the basal condition, and it is likely that the α7 nAChR subunit is dominant in cultured hippocampal neurons. In contrast to the effect of nicotine, the redistribution of VILIP-1 mediated by NMDARs evoked by glutamate/glycine was not attenuated by either MLA or MLA/DHβE compared with the control, suggesting nAChR, and NMDAR can contribute to an increase of Ca^{2+} in hippocampal neurons.

These results indicate that an increase in the intracellular calcium concentration after neuronal activity can induce a rapid translocation of VILIP-1 to membranes in hippocampal neurons, and this calcium-induced localization is reversible. Therefore, the calcium-myristoyl switch mechanism enables VILIP-1 to dynamically shuttle between different cellular compartments. Therefore VILIP-1 can probably reversibly interact with putative interaction partners, such as signal effector proteins, in distinct membrane compartments.

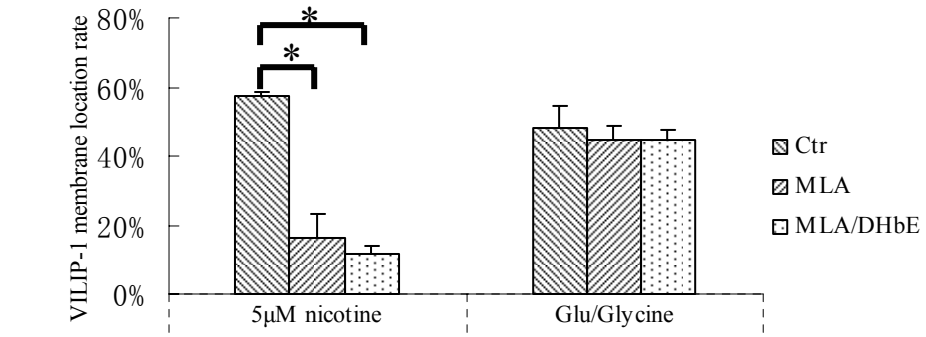

	5µM nicotine	Glu/Glycine
Ctr	57,6%	48,3%
MLA	16,4%	44,5%
MLA/DHbE	11,7%	44,9%

Figure 14 Quantification of the nicotine-induced membrane distribution of endogenous VILIP-1 and the blockade of this effect by MLA and DHβE in comparison to the glutamate/glycine stimulation. Graphs and error bars represent mean value and S.E.M., respectively, of results obtained from three experiments.

5. VILIP-1 affects responsiveness of α4β2 nAChR to ACh in transiently and stably transfected HEK cells

Lin et al. (Lin et al., 2002) have shown that VILIP-1 interacted with the α4 nAChR subunit, and enhanced surface expression of α4β2 nAChR in transiently VILIP-1 and α4β2 nAChR cotransfected oocytes. To test whether the effect of VILIP-1 on the surface expression of α4β2 nAChR also leads to functional up-regulation of the expressed receptor, I performed whole-cell patch-clamp studies (Fig. 15). First, recordings from α4β2 nAChR receptor and GFP or VILIP-1-GFP-cotransfected HEK cells and from GFP or VILIP-1-GFP-transfected HEK cells stably expressing the human α4β2 nAChR (cell line Hα4β2 Lx/1) were analyzed (cells with moderate level of GFP intensity were selected for experiment). ACh evoked current with a slow component at a saturating concentration of 3mM ACh, which could be completely blocked by 100nM DHβE, an antagonist of α4β2 nAChR, indicating that it is subserved by the functional α4β2 nAChR present in the Hα4β2Lx/1 cell lines ectopically expressing the human α4β2 nAChR. Following washout of the antagonist, the current could be partially recovered (Fig. 15 A, upper panel). These data are comparable to those previously reported (Samochocki et al., 2000, 2003). Similar results, but relatively smaller amplitudes, were obtained using transiently transfected HEK-293 cells (data not shown). Under the same saturation conditions (3 mM ACh) the response to ACh was significantly increased in amplitude in the VILIP-1-GFP co-transfected cells compared to the responses in GFP-transfected HEK cells expressing human α4β2 nAChR (Fig. 15 A, compare representative traces in red, VILIP-1-GFP, and black, GFP).These results indicate that VILIP-1 not only increases surface expression but at the same time increases the responsiveness of cells expressing the rat and human α4β2 nAChR for its ligand ACh.

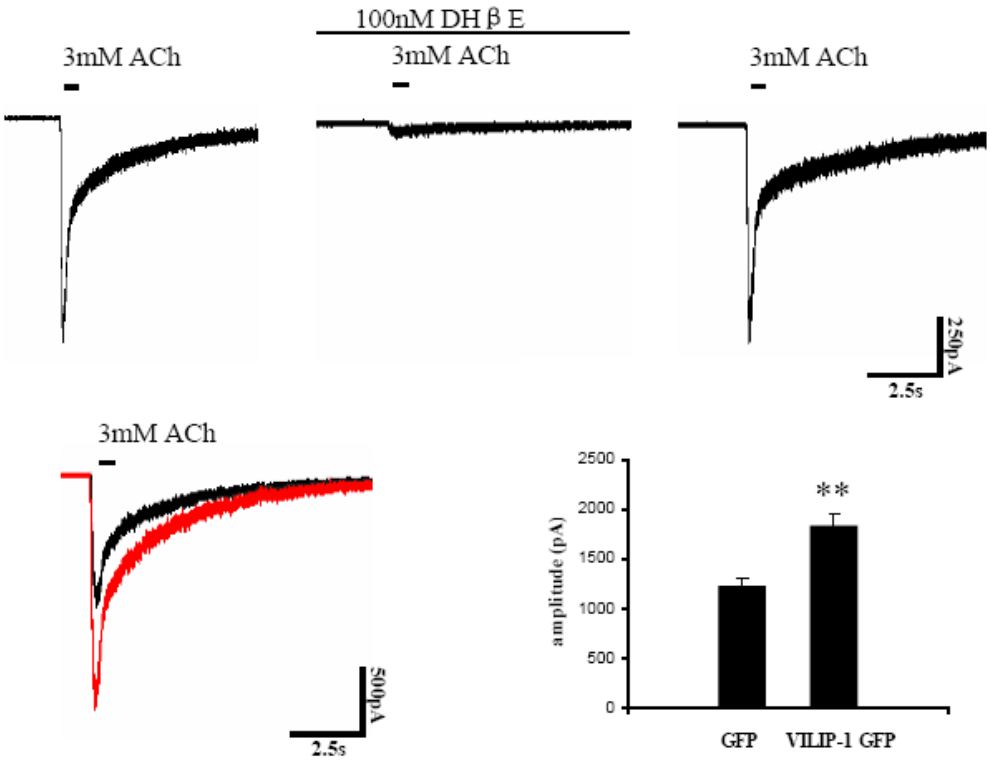

Figure 15 Potentiation of acetylcholine-induced whole-cell responses by VILIP-1 recorded from HEK-293 cells expressing human α4β2 nAChR.
Whole-cell responses to ACh, in the absence and presence of 100nM DHβE, were recorded from a single cell of cell line H α4β2 Lx/1, which was held at -60mV. ACh concentrations applied were in the range of saturation responses. ACh evoked current could be blocked by 100nM DHβE completely (second trace), which is an antagonist of alpha4 beta2 nAChR; the current could be recovered after DHβE was washed out. Representative traces of whole-cell responses from GFP transfected cell (black trace), and VILIP-1-GFP transfected cell (red trace) at 3mM ACh concentration are shown in left panel. The response to ACh in the VILIP-1-GFP transfected cells (n=33, from two different preparations) is highly significantly increased in amplitude ($p<0.01$), as compared to the responses to ACh in GFP transfected cells (n=18, from two different experiments).

6. VILIP-1 affects responsiveness of α4β2 nAChR to ACh in transfected hippocampal neurons

I further investigated primary hippocampal neurons which expressed the cotransfected α4β2 nAChR and GFP or VILIP-1-GFP (cells with moderate level of GFP intensity were selected for measurement). Nicotinic currents were isolated by blocking GABAergic, glutamatergic and muscarinergic transmission with bicuculline, CNQX, TTX, APV and atrophine. At saturation conditions (3 mM ACh) the ACh evoked current with slow kinetic inactivation could be blocked by 100nM of the receptor antagonist DHβE (Fig. 16 B, upper panel), and partially recovered after washout. These currents resembled type II nAChR currents which are typical for α4β2 nAChRs (Alkondon and Albuquerque, 1993, 1995; Albuquerque et al., 1997). The amplitude and kinetic properties of ACh evoked current is similar to the transient transfected α4β2 nAChR in midbrain neuron culture (Nashmi et al., 2003). VILIP-1-GFP caused a significant increase in the amplitude of

ACh currents compared to GFP-controls (Fig. 16 B, compare representative traces in red, VILIP-1-GFP, and black, GFP). Interestingly, there was some variation observed in the magnitude of the responses. Plotting the amplitude against the deviation of average identified a group of neurons as high ACh responders with about 2.5 fold higher amplitude current than the second group of low responders (data not shown). The group of high responders might indicate a strong basal expression of α4β2 nAChR, for example, in certain types of interneurons in the hippocampal formation. These results support the notion that enhanced VILIP-1 expression leads to functional up-regulation of α4β2 nAChR in hippocampal neurons.

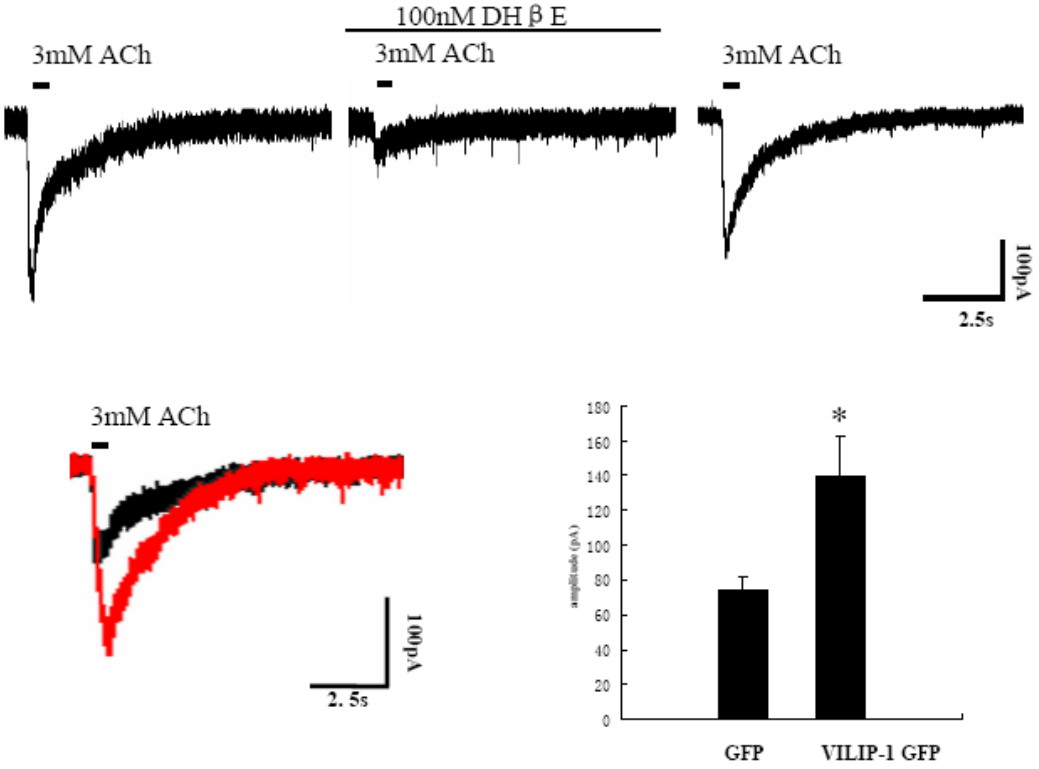

Figure 16 Potentiation of acetylcholine-induced whole-cell responses by VILIP-1 recorded from hippocampal cultured cells expressing rat α4β2 nAChR.
Whole-cell responses to ACh, in the absence and presence of 100nM DHβE, were recorded from a single cell of cultured hippocampal neuron, which was held at -70mV. ACh concentrations applied were in the range of saturation responses. ACh evoked current could be blocked by 100nM DHβE (second trace), which is an antagonist of α4β2 nAChR; the current could be partially recovered after DHβE was washed out. Representative traces of whole-cell responses from α4β2 nAChR, GFP constructs co-transfected cell (black trace), and α4β2 nAChR, VILIP-1-GFP constructs co-transfected cell (red trace) under 3mM ACh concentration are shown in the left panel. The response to ACh in the VILIP-1-GFP transfected cells (n=13, from two different experiments) is highly significantly increased in amplitude ($p < 0.05$), as compared to the responses to ACh in GFP transfected cells (n=14, from 3 different experiments).

7. Comparison of the effect of α4β2 nAChR activation on inhibitory postsynaptic currents (IPSCs) recorded from GFP control and GFP-VILIP-1 transfected hippocampal neuronal cultures.

To investigate whether VILIP-1 modulates inhibitory postsynaptic currents (IPSCs) in hippocampal neuron cultures, whole-cell patch-clamp recording was performed in neurons which were located in close proximity to either VILIP-1-GFP or GFP alone transfected hippocampal neurons visualized by fluorescence microscopy. IPSCs can be recorded from cultured hippocampal neurons when CNQX is present in the recording solution and are mediated by GABA released from spontaneously firing neurons that synapse onto the neurons from which recordings are obtained. These currents are herein referred to as IPSCs and can be blocked completely by application of 30μM bicuculline (data not shown). In all experiments D-AP5, CNQX, 5 nM MLA, and 1μM atrophine were included in the external solution; therefore, under our experimental conditions the contribution of α7 nACh receptors and muscarinic acetylcholine receptors (mAChR) to GABAergic synaptic events is negligible. Both varied frequency and amplitude of spontaneous IPSCs were similar in both groups. 10μM ACh was applied using bath application for 1 minute after recording of a stable baseline for 1-2 minutes, and then washed out. In both VILIP-1-GFP and GFP-transfected cultures, 10μM ACh evoked an increase in the number of IPSC events, with bursts of IPSCs which can be seen occasionally, compared to baseline recordings (Fig. 17 B). This was true when neurons were held at different voltages (data not shown). Furthermore, the ACh evoked IPSCs were blocked by the application of 30μM bicuculline and partially recovered after bicuculline was washed out for 1 minute (Fig. 17 A). Maria et al. demonstrated that stimulation with ACh via both, α7 nAChR and α4 nAChR, contributed to enhance IPSCs in hippocampal neuron culture. However, the effect of α4 nAChR was dominant, since the α4 nAChR-specific inhibitor DHβE could block about 65% of the ACh effect (Maria et al., 2004). Thus, the ACh-triggered IPSCs in the current experiments were likely the result of the interaction of the agonist with α4β2 nAChRs present in neurons synapsing onto the neurons under study. Interestingly, more ACh mediated IPSCs events, as well as larger IPSC amplitudes, were found in VILIP-1-GFP transfected neurons compared to GFP-transfected neurons (Fig. 17 B). Quantification of frequency data (Fig. 17 C) demonstrated that there were indeed higher frequencies of IPSCs in the VILIP-1-GFP transfected neurons at time points 120,180, 240, and 300 seconds, which reached with a two-fold increase of frequency the level of highly significance at the time point 180 seconds (normalized to baseline recording), compared to GFP-transfected neurons. The cumulative amplitude was clearly different between the two recorded groups, indicating that more events with bigger amplitude were present in the VILIP-1 group; however, the average amplitude of the IPSCs of the two groups showed no significant difference, which might be due to more small events occurring in the VILIP-1 group (Fig. 17 D).

These findings suggest that 10µM ACh is efficient not only to enhance IPSCs frequency but also amplitude in VILIP-1-GFP-transfected hippocampal neuronal culture. Considering that 5nM MLA and 1µM atrophine were included in the external recording solution, the effect is most likely due to a presynaptic mechanism via stimulation of non-α7 nAChR, and therefore most likely via α4 nAChRs. Together with the finding of the interaction between VILIP-1 and the α4 nAChR subunit, these results further suggest that VILIP-1 enhances functional α4 nAChR expression in presynaptic terminals in certain interneurons of hippocampal culture, which therefore leads to an enhancement of ACh-triggered IPSCs. However, the contribution of postsynaptic VILIP-1-dependent mechanisms can not be excluded completely.

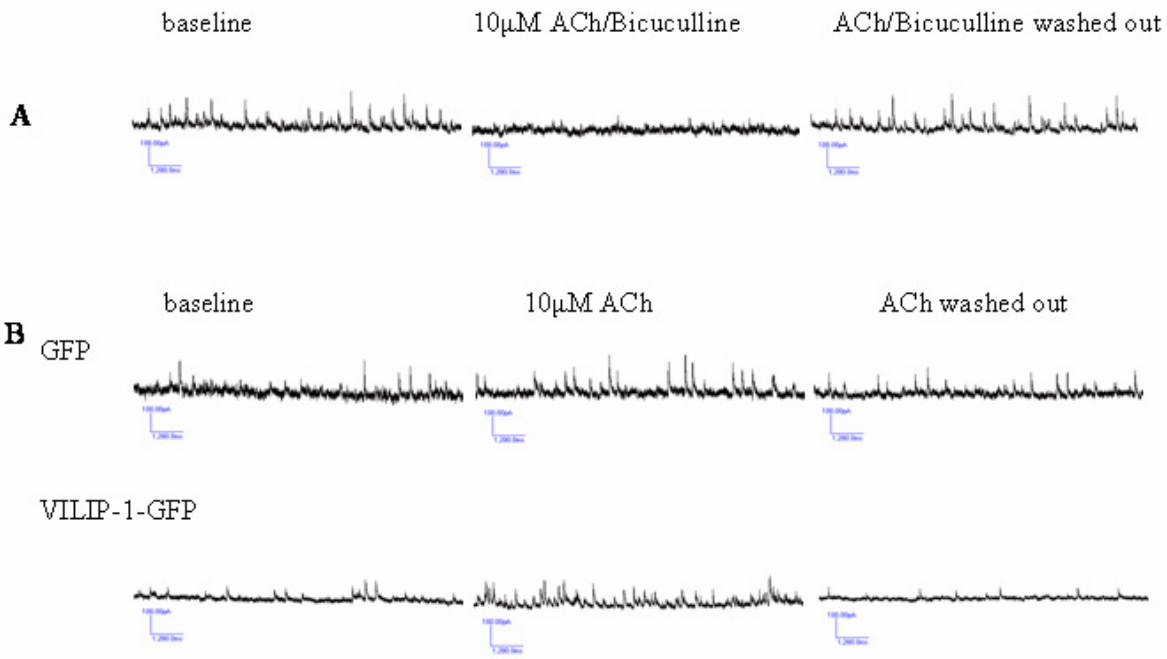

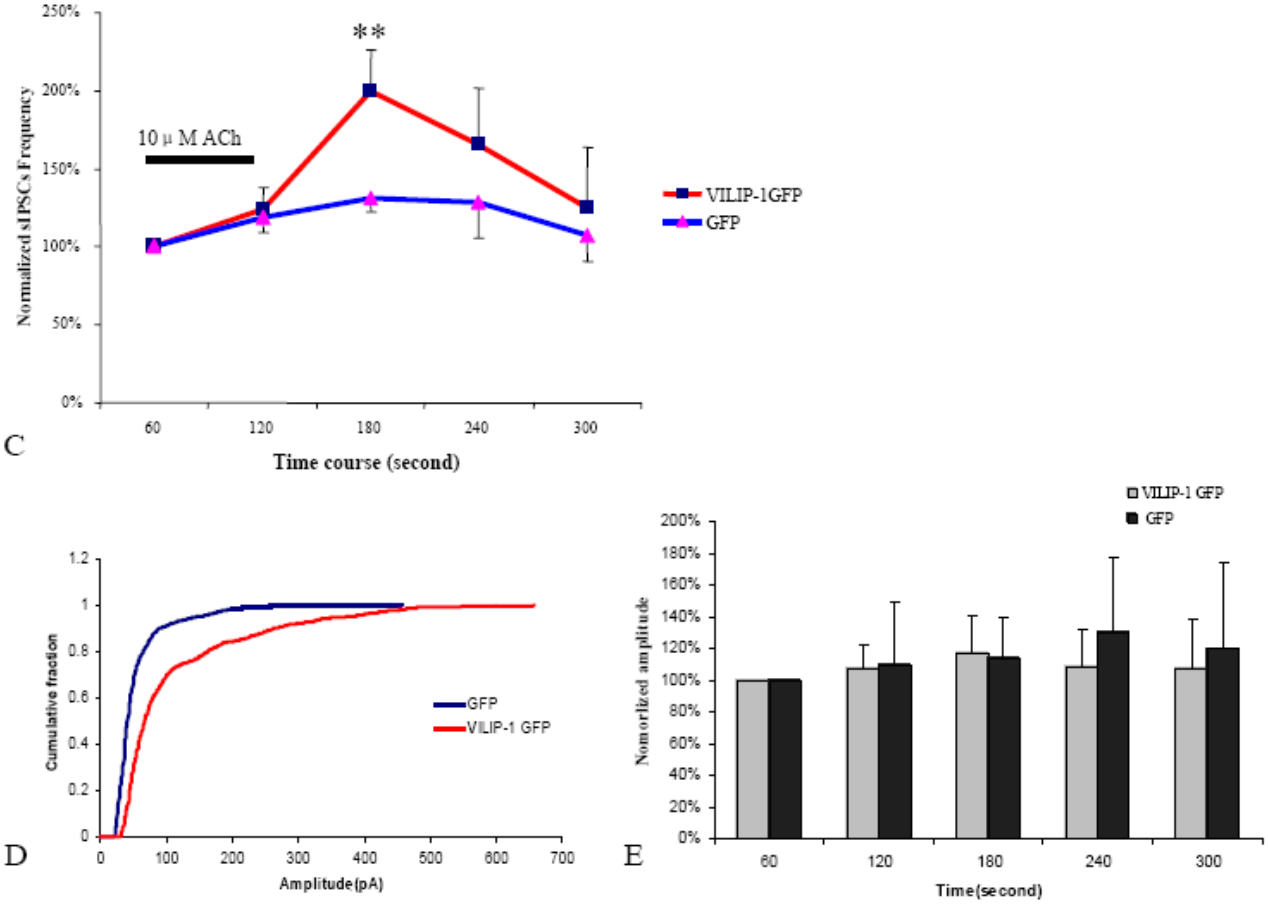

Figure 17 Characterization and comparison of ACh-triggered IPSCs.
A.**)** Sample recordings of IPSCs obtained from a cultured hippocampal neuron, which was held at -10mV. Recorded IPSCs were blocked by bicuculline and partially recovered after washing out for 2 minutes. **B**.) Sample traces recorded in a GFP–transfected neuron and in VILIP-1-GFP transfected neuron showing IPSC frequency evoked by bath application of ACh (10 μM) to nearby neurons synapsing onto the neuron under study. **C.)** Quantification of the ACh-induced enhancement of the IPSC frequency in the GFP transfected group (n=8) and in the VILIP-1-GFP transfected group (n=14). Under each experimental condition, the baseline frequency of IPSCs was taken as 1 and used to normalize the frequency of IPSCs triggered by ACh (10μM). Graph and error bars represent mean and S.E.M., respectively. ** $p< 0.01$ according to the Student's *t* test. **D)**. Cumulative amplitude of IPSCs in GFP group (n=4) and in VILIP-1-GFP transfected neurons (n=8) from the same preparation. **E).** Average amplitude of IPSCs in the GFP group and in the VILIP-1-GFP transfection group from the same preparation as in D. Under each experimental condition, the baseline average amplitude of IPSCs was taken as 100% and used to normalize the average amplitude of IPSCs triggered by ACh (10μM). Graph and error bars represent mean and S.E.M., respectively.

8. Time-dependent upregulation of VILIP-1 and NCS-1 expression following application of DHPG in the hippocampus *in vivo*

Modulation of IPSCs of cultured hippocampal neurons *in vitro*, together with increasing VILIP-1 in a subpopulation of interneurons of the hippocampus, and decreasing in pyramidal cells of hippocampal CA1 in the brains of schizophrenic patients and ketamine treated rats suggest that VILIP-1 might be involved in hippocampal network activities, therefore we studied the expression of VILIP-1 in synaptic plasticity model *in vivo*, DHPG induced slow onset

potentiation in rat hippocampus, by using Western blot analysis.

Application of DHPG leads to increased VILIP-1 expression in the hippocampus already after 2 and 4 h but higher levels were reached at 8 and 24 h (Fig. 19 A, VILIP-1, $n = 2$ for time points 2, 4, and 8 h; $n = 3$ for control and 24 h) following drug injection. For comparison, we analyzed NCS-1, a calcium sensor protein shown to be involved in short term plasticity (Sippy et al., 2004). Similarly, increased expression of NCS-1 protein occurred at 2 and 4 h but reached strongest levels after 8 and 24 h (Fig. 19 A, NCS-1, $n = 2$ for time points 2, 4, and 8 h; $n = 3$ for control and 24 h) after DHPG treatment. Quantification of the Western blot data revealed significant increases in the relative expression level of VILIP-1 and NCS-1 at 8 and 24 h following drug application in the hippocampus *in vivo* (Fig. 19 C and D). Thus, a DHPG concentration sufficient to induce synaptic plasticity in the form of slow onset potentiation in the rat hippocampus *in vivo* (Braunewell et al., 2003) leads to an increase of NCS protein expression reaching significant levels at 8 and 24 h following drug application.

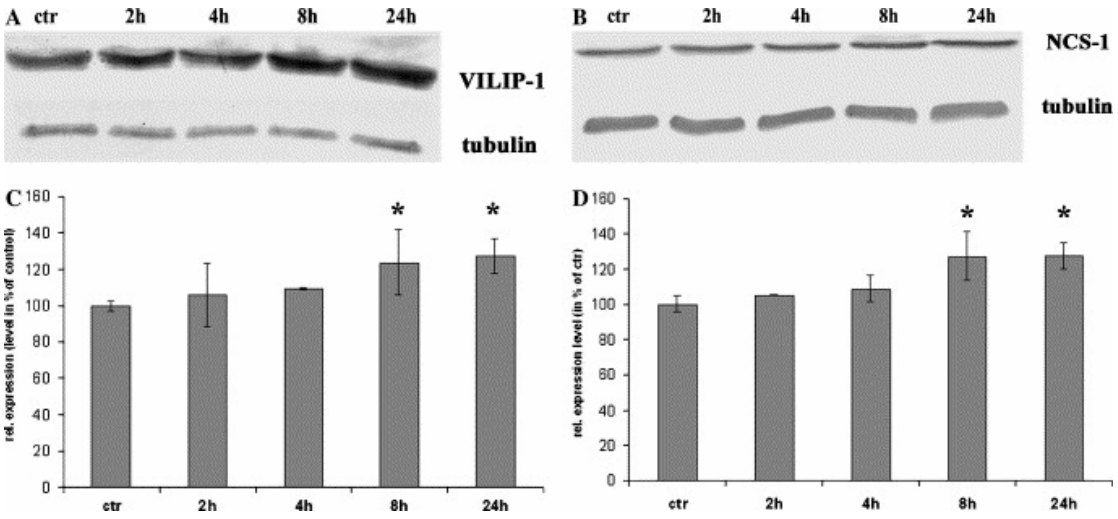

Figure 18 Western blot analysis of homogenates of hippocampi which have been treated *in vivo* with vehicle or with the group I mGluR agonist DHPG for 2, 4, 8, and 24 h using specific antibodies against the NCS proteins (A) VILIP-1 and (B) NCS-1.
Quantification of Western blot analysis of homogenates of hippocampi which have been treated with the group I mGluR agonist DHPG for 2, 4, 8, and 24 h using specific antibodies against the NCS proteins (C) VILIP-1 and (D) NCS-1. Control expression without treatment was set to 100%. Mean values ± SD are from two independent experiments ($n = 2$) for time points 2, 4, and 8 h; and three independent experiments ($n = 3$) for control and time point 24 h each carried out twice. Data were analyzed by ANOVA with post hoc Fisher's PLSD. Asterisks (*) show significant differences.

9. Intrinsic electrophysiological properties of VILIP-1 transfected hippocampal neurons

To investigate the physiological effect of VILIP-1 overexpression in hippocampal neuronal cultures, a modified transfection protocol for physiological measurement and whole-cell patch clamp recordings were established. The hippocampal cells about 2-4h after dissociation were

small and spherical, with a mean diameter of about 8 µm. The isolated cells, which were attached directly to the substrate, have extended one or two unbranched neurites. The nerve cells continued to extend processes within the following days in culture. Most of the cultures survived for more than three weeks. The neuronal population in these cultures is heterogeneous and includes hippocampal areas CA1 and CA3 pyramidal neurons, dentate gyrus granule cells and interneurons. Different types of neuronal cell types could be seen in hippocampal cultures: pyramidal, stellate and basket cells. In order to minimize electrophysiological heterogeneity: cells were phase bright, over 10 µm in diameter with smooth appearing somas with one or more small dendrites and a large apical dendrite, with second order dendrites branching from it after 10-14days in culture. Morphologically, the neurons selected resembled pyramidal neurons, but could have other origins.

Table 2 Functional properties of VILIP-1 in hippocampal neurons

Group / Parameter	Control cells	VILIP-1 transfected cells
Resting potential	-59.3±11.2 mV	-61.9±5.18 mV
Input resistance	243.1±65 MΩ	279.7±99 MΩ
Time constant	23.13±7.8ms	24.95±6.95ms
Action potentials height	97.3±14.2 mV	96.8±13.2mV
Action potentials duration	1.84±0.31 ms	2.49±0.73ms (significant difference)

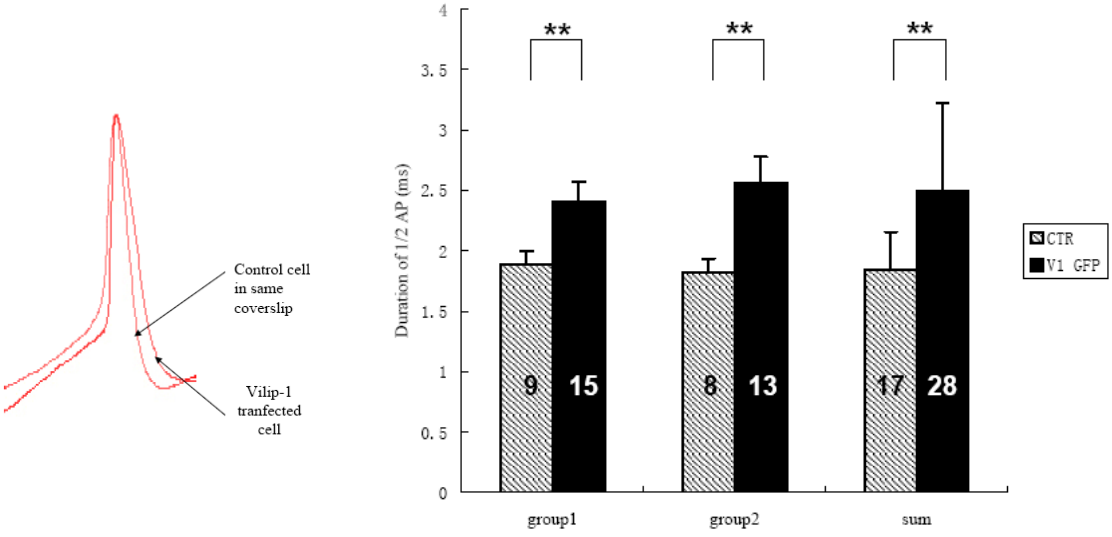

Figure 19. VILIP-1 alters the half duration of the action potential compared with control neurons. Representative action potentials form VILIP-GFP cell and control cell as indicated are shown in left graph. The histogram of the half duration of action potential from 2 sets of experiment is shown in the right graph. The numbers of measured cells in each group are shown as indicated. Asterisks (*) show significant differences.

To overexpress VILIP-1, VILIP-1-GFP was transiently transfected in cultured hippocampal neurons. After 1-2 days following transfection, the pyramidal shaped neurons labeled with moderate level of GFP fluorescence intensity were selected and measurements were performed.

The intrinsic properties were investigated and compared with neighboring neurons with similar morphological characteristics. Cells with membrane potentials more than -40 mV were not considered viable or had a bad seal and were thus eliminated from the analysis. This number was chosen as the cut-off, because cells with membrane potentials more than -40 mV were never found to produce a true action potential, even when current was injected to hyperpolarize the cell. Cells with membrane potentials less than -40 mV were usually capable of producing an overshooting action potential when the cell was hyperpolarized. Prior to the introduction of any depolarizing pulses, current was injected when necessary to bring the membrane potential to between -55 and -65mV in order to be able to compare different cells and to insure that the sodium channels contributing to the action potential were not inactivated. An ANOVA was performed for input resistance, time constant, action potential amplitude, resting membrane potential, maximum number of action potentials fired in response to a 100-ms depolarizing pulse. There were no significant differences between the input resistance, action potential amplitude, and time constant between the two groups (Table 2). However, action potentials with longer duration were seen in VILIP-1-transfected hippocampal neurons compared to control cells. VILIP-1 altered the half duration of the recorded action potentials significantly in 2 sets of experiment (Fig 19, n=2, number of neurons was 17 for control, 28 for VILIP-1-GFP group). No other significant differences in intrinsic properties were found between the two groups.

Thus, VILIP-1 alters the half duration of the action potential in cultured hippocampal neurons, which suggests VILIP-1 might modulate the synaptic transmission by shaping the action potential (Wheeler et al., 1996). However, the molecular targets and the precise mechanisms underlying the VILIP-effect still have to be revealed.